SIAM J. SCI. COMPUT.
Vol. 0, No. 0, pp. 000–000

ADJOINT-BASED A POSTERIORI ERROR ESTIMATION FOR COUPLED TIME-DEPENDENT SYSTEMS*

LIYA ASNER†, SIMON TAVENER‡, AND DAVID KAY§

Abstract. We consider time-dependent parabolic problems coupled across a common interface which we formulate using a Lagrange multiplier construction and solve by applying a monolithic solution technique. We derive an adjoint-based a posteriori error representation for a quantity of interest given by a linear functional of the solution. We establish the accuracy of our error representation formula through numerical experimentation and investigate the effect of error in the adjoint solution. Crucially, the error representation affords a distinction between temporal and spatial errors and can be used as a basis for a blockwise time-space refinement strategy. Numerical tests illustrate the efficacy of the refinement strategy by capturing the distinctive behavior of a localized traveling wave solution. The saddle point systems considered here are equivalent to those arising in the mortar finite element technique for parabolic problems.

Key words. coupled problem, a posteriori error analysis, mesh refinement, adjoint problem, mortar finite elements

AMS subject classifications. 65N15, 65N30, 65N50

DOI. 10.1137/110858458

1. Introduction.

We consider an adjoint-based a posteriori error estimator for parabolic problems that are coupled across a given interface and construct an adaptive space-time finite element scheme. A posteriori error estimation is commonly used in parabolic problems for adaptive mesh refinement and the different approaches are described in a detailed review paper [1], as well as in [4, 5, 14, 20, 24, 35, 39, 40, 41]. In particular, [14, 15, 16] develop a technique based on solving an adjoint problem to estimate the error in a quantity of interest given by a functional of the solution as opposed to the error in a norm of the solution.

Error estimation for coupled problems solved using operator decomposition techniques was considered in [17, 18, 9, 8]. While operator decomposition is traditionally viewed as easy and inexpensive to implement [19, 28], its convergence is rarely guaranteed. In this paper we take the alternative, monolithic approach to solving coupled parabolic problems, which do not suffer from this problem. We introduce a Lagrange multiplier (mortar element) space on the interface between the component domains, resulting in a large-scale complex system, which can nevertheless be solved efficiently with special treatment [33, 22]. Moreover, the presence of the Lagrange multiplier variable allows us to derive error estimates for a quantity of interest that is supported along the interface. This is particularly useful in applications where the Lagrange

*Submitted to the journal's Methods and Algorithms for Scientific Computing section December 9, 2011; accepted for publication (in revised form) May 30, 2012; published electronically DATE. This work was supported in part by award KUK-C1-013-04, made by King Abdullah University of Science and Technology (KAUST).

http://www.siam.org/journals/sisc/x-x/85845.html

†Department of Computer Science, University of Oxford, OX1 3QD, Oxford, UK (liya.asner@comlab.ox.ac.uk). This author's work is supported by the Clarendon Fund, University of Oxford and by the Scatcherd European Scholarship.

‡Department of Mathematics, Colorado State University, Fort Collins, CO 80523 (tavener@math.colostate.edu).

§Department of Computer Science, University of Oxford, OX1 3QD, Oxford, UK (david.kay@comlab.ox.ac.uk).

multiplier represents an important physical quantity. Similar systems arise when using mortar elements [7, 2, 3, 6] as part of a domain decomposition approach [34] to solving elliptic or parabolic systems.

Multiphysics problems in which the coupling occurs across a common interface arise in many fields. For example, models of fluid-structure interaction are of interest in many physiological applications [12, 23, 26, 38]. Examples include the normal stress along arterial walls when assessing the risk of aneurysm rupture [12, 11], and the flux through the boundary between a fluid and a porous media when modeling air flow in the lungs [27]. The problems considered here are a necessary step towards an a posteriori error analysis for more complicated multiphysics systems.

Recent investigations [29, 25] have established convergence of goal-oriented adaptive schemes for linear and nonlinear parabolic problems, respectively, and build on the earlier work of [31, 30]. These analyses require a Dörfler "mark and refine" strategy [13] and simultaneously refine both forward and adjoint problems. The extension of the approach in [29, 25] to goal-oriented adaptivity for coupled parabolic systems such as those studied here is not immediate. Our focus is on error estimation and on a single refinement step. We do not attempt to prove the convergence of our adaptive strategy. Nor do we seek to develop methods akin to the "safeguarded" dual weighted residual method of [32] that allow for inaccuracy in the (numerical) adjoint solution.

The structure of this paper is as follows. We formulate a coupled time-dependent problem in section 2 and define our solution method. In section 3 we introduce the error in the quantity of interest and derive an error representation formula. We also assess its accuracy in the presence of an inexact adjoint solution. A blockwise adaptive mesh refinement strategy is then discussed in section 4. The effectivity of the error estimator is demonstrated in section 5. Finally, section 6 illustrates the performance of the mesh refinement algorithm.

2. A model coupled time-dependent problem. Our model problem is to find functions $u_i(x,t)$, $x \in \Omega_i$, $t \in [0,T]$, for $i = 1,2$, where Ω_i are nonoverlapping open polygonal domains sharing a common interface Γ. Here, $u_1(x,t)$ and $u_2(x,t)$ satisfy the following partial differential equations, continuity constraints along Γ, and initial and boundary values:

$$\frac{\partial u_i}{\partial t} + \mathcal{L}_i u_i = f_i \qquad \text{in } \Omega_i \times (0,T], \quad i = 1,2, \tag{2.1}$$

$$u_i(x,0) = u_{i,0}(x) \qquad \forall x \in \Omega_i, \quad i = 1,2, \tag{2.2}$$

$$u_i = u_i^D \qquad \text{on } \Gamma_i^D \times (0,T], \quad i = 1,2, \tag{2.3}$$

$$k_i \frac{\partial u_i}{\partial n_i} = 0 \qquad \text{on } \Gamma_i^N \times (0,T], \quad i = 1,2, \tag{2.4}$$

$$u_1 = u_2 \qquad \text{on } \Gamma \times (0,T], \tag{2.5}$$

$$k_1 \frac{\partial u_1}{\partial n_1} = -k_2 \frac{\partial u_2}{\partial n_2} \qquad \text{on } \Gamma \times (0,T], \tag{2.6}$$

where $\mathcal{L}_i u_i = -\nabla \cdot (k_i \nabla u_i) + c_i u_i$, $k_i \geq k_{i,0} > 0$, c_i and f_i are sufficiently smooth, and the domain boundaries $\partial\Omega_i = \Gamma_i^D \cup \Gamma_i^N \cup \Gamma$, $i = 1,2$, are such that $\Gamma_i^D \cap \Gamma_i^N = \emptyset$, $\Gamma_i^D \cap \Gamma = \emptyset$, and $\Gamma_i^N \cap \Gamma = \emptyset$.

In order to construct weak solutions, we introduce the function spaces $X_i = L_2(0,T;H^1(\Omega_i))$, $i = 1,2$, and $Y = L_2(0,T;H^{-1/2}(\Gamma))$. We also let

$$X_{i,D} := \{v \in X_i \mid v = u_i^D \ \text{ on } \Gamma_i^D \times I\}, \quad i = 1,2,$$
$$X_{i,0} := \{v \in X_i \mid v = 0 \ \text{ on } \Gamma_i^D \times I\}, \quad i = 1,2,$$

be the affine subspaces including the given Dirichlet and zero Dirichlet boundary conditions, respectively, along Γ_i^D.

For any $v_i, w_i \in X_i$, $i = 1,2$, we define the following bilinear forms:

$$(v_i, w_i) := \int_{\Omega_i} v_i w_i \ \mathrm{d}x, \quad a_i(v_i, w_i) := \int_{\Omega_i} (k_i \nabla v_i \cdot \nabla w_i + c_i v_i w_i) \ \mathrm{d}x.$$

Finally, for any pair $(v, \nu) \in X_i \times Y$ we define $< \nu, v >$ to be the standard duality pairing. Note, we assume the action of the trace operator on v is contained within the duality pairing.

The weak form of (2.1)–(2.6) is as follows: *Find* $(u_1, u_2, \lambda) \in X_{1,D} \times X_{2,D} \times Y$ *such that*

$$\int_0^T \left\{ \mp < \lambda, v_i > + \left(\frac{\partial u_i}{\partial t}, v_i \right) + a_i(u_i, v_i) - (f_i, v_i) \right\} \ \mathrm{d}t = 0$$
$$\forall v_i \in X_{i,0}, \quad i = 1,2, \tag{2.7}$$

$$\int_0^T < \nu, u_1 - u_2 > \ \mathrm{d}t = 0 \ \forall \nu \in Y, \tag{2.8}$$

$$u_i(x,0) = u_{i,0}(x), \quad i = 1,2. \tag{2.9}$$

In the first equation we use shorthand notation $\mp < \lambda, v_i >$, $i = 1,2$, for the terms $- < \lambda, v_1 >$ when $i = 1$, and $< \lambda, v_2 >$ when $i = 2$. In the text below the top sign always corresponds to $i = 1$ and the bottom sign to $i = 2$.

Note. Nonzero Neumann boundary conditions on Γ_i^N, $i = 1,2$, will result in additional boundary integral terms in (2.7).

We construct a finite element method for this problem using continuous piecewise-linear functions in space (cG(1) in space) and discontinuous piecewise-constant functions in time (dG(0) in time). We denote the spatial and temporal discretization spaces by P_c^1 and P_d^0, respectively. First, we partition $I = (0,T]$ into N time intervals, $0 = t_0 < t_1 < \cdots \leq t_N = T$ with $\Delta t_n = t_n - t_{n-1}$ and define $I_n = (t_{n-1}, t_n]$. We construct regular triangulations τ_i for Ω_i, $i = 1,2$, and a partition τ for Γ, consisting of nonoverlapping elements Δ and γ, respectively. The corresponding finite element spaces are

$$X_i^h := \{v \in X_i \mid v(\cdot,t) \in P_c^1(\tau_i) \ \forall t \in I, \ v(x,\cdot) \in P_d^0(\{I_n\}) \ \forall x \in \Omega_i\}, \quad i = 1,2,$$
$$Y^h := \{\nu \in Y \mid \nu(\cdot,t) \in P_c^1(\tau) \ \forall t \in I, \ \nu(s,\cdot) \in P_d^0(\{I_n\}) \ \forall s \in \Gamma\},$$

with subspaces $X_{i,D}^h = X_i^h \cap X_{i,D}$ and $X_{i,0}^h = X_i^h \cap X_{i,0}$, $i = 1,2$. We define semi-discrete subspaces of the test spaces X_1, X_2, and Y, and the projections π^h and θ

onto these semidiscrete subspaces as

$$
\begin{aligned}
X_i^x &:= \{v \in X_i \mid v(\cdot,t) \in P_c^1(\tau_i)\ \forall t \in I\}, \quad i = 1,2,\\
Y^x &:= \{\nu \in Y \mid \nu(\cdot,t) \in P_c^1(\tau)\ \forall t \in I\},\\
X_i^t &:= \{v \in X_i \mid v(x,\cdot) \in P_d^0(\{I_n\})\ \forall x \in \Omega_i\}, \quad i = 1,2,\\
Y^t &:= \{\nu \in Y \mid \nu(s,\cdot) \in P_d^0(\{I_n\})\ \forall s \in \Gamma\},\\
\pi^h &: \begin{cases} X_i \to X_i^x & \text{such that } \forall v \in X_i,\ w \in X_i^x :\ (v - \pi^h v, w) = 0, \quad i = 1,2,\\ Y \to Y^x & \text{such that } \forall \nu \in Y,\ w \in X_j^x : < \nu - \pi^h \nu, w >= 0, \end{cases}\\
\theta &: \begin{cases} X_i \to X_i^t & \text{such that } \forall v \in X_i,\ w \in X_i^t :\ (v - \theta v, w) = 0, \quad i = 1,2,\\ Y \to Y^t & \text{such that } \forall \nu \in Y,\ w \in X_j^t : < \nu - \theta \nu, w >= 0, \end{cases}
\end{aligned}
$$

where j is the index of the domain that defines the finite element space on Γ (i.e., that where the mesh in the domain conforms with the mesh on the interface). Finally, let $[u_i^h]_n = \lim_{t \downarrow t_n} u_i^h(t) - \lim_{t \uparrow t_n} u_i^h(t)$ denote the jumps in the (discontinuous in time) finite element solutions u_i^h at times t_n.

The resulting finite element method can be written as follows: *Find* $(u_1^h, u_2^h, \lambda^h) \in X_{1,D}^h \times X_{2,D}^h \times Y^h$ *such that*

$$
\sum_{n=1}^{N} \left\{ \left(\left[u_i^h\right]_{n-1}, v_{i,(n-1)+}^h \right) - \int_{I_n} (R_i, v_i^h)\ \mathrm{d}t \right\} = 0 \quad \forall v_i^h \in X_{i,0}^h, \quad i = 1,2, \tag{2.10}
$$

$$
\sum_{n=1}^{N} \int_{I_n} < \nu^h, u_1^h - u_2^h >\ \mathrm{d}t = 0 \quad \forall \nu^h \in Y^h, \tag{2.11}
$$

$$
u_i^h(x,0) = \pi^h u_{i,0}(x), \quad i = 1,2, \tag{2.12}
$$

where R_1 and R_2 are the residuals

$$
(R_i, v_i) = \pm < \lambda^h, v_i > + (f_i, v_i) - \left(\frac{\partial u_i^h}{\partial t}, v_i \right) - a_i(u_i^h, v_i) \quad \forall v_i \in X_i^h, \quad i = 1,2. \tag{2.13}
$$

For sufficiently smooth interfaces the problem is known to be well posed [21]. Interfaces with corners require a more precise definition of the Lagrange multiplier space.

3. The error representation formula. Let the discretization errors be defined as $e_i = u_i - u_i^h$, $i = 1,2$, and $e_\lambda = \lambda - \lambda^h$, which are functions of both space and time. The quantity of interest

$$
(QoI) = \int_0^T \{- < \lambda, \psi > + (u_1, \psi_1) + (u_2, \psi_2)\}\ \mathrm{d}t, \tag{3.1}
$$

is a linear functional of the solution with coefficients ψ_1, ψ_2, and ψ, and has error

$$
\mathcal{E} = \int_0^T \{- < e_\lambda, \psi > + (e_1, \psi_1) + (e_2, \psi_2)\}\ \mathrm{d}t. \tag{3.2}
$$

The adjoint problem corresponding to (2.7)–(2.8) is as follows: *Find* $(\phi_1, \phi_2, \mu) \in X_{1,0} \times X_{2,0} \times Y$ *such that*

$$\int_0^T \left\{ \mp < \mu, v_i > - \left(\frac{\partial \phi_i}{\partial t}, v_i \right) + a_i(\phi_i, v_i) - (\psi_i, v_i) \right\} \, \mathrm{d}t = 0$$

$$\forall v_i \in X_{i,0}, \quad i = 1, 2, \tag{3.3}$$

$$\int_0^T < \rho, \phi_1 - \phi_2 > \, \mathrm{d}t = \int_0^T < \rho, \psi > \, \mathrm{d}t \quad \forall \rho \in Y, \tag{3.4}$$

$$\phi_i(x, T) = 0, \quad i = 1, 2. \tag{3.5}$$

THEOREM 3.1. *The error* $\mathcal{E}$ *defined by* (3.2) *can be computed as*

$$\mathcal{E} = \sum_{i=1}^{2} \left\{ (\phi_{i,0}, u_{i,0} - \pi u_{i,0}) - \sum_{n=1}^{N} (\phi_{i,n-1}, [u_i^h]_{n-1}) \right.$$
$$\left. + \sum_{n=1}^{N} \int_{I_n} \left\{ \pm < \mu, u_i^h > + (R_i, \phi_i) \right\} \, \mathrm{d}t \right\}, \tag{3.6}$$

where (ϕ_1, ϕ_2, μ) *is the solution of the adjoint problem* (3.3)–(3.5) *and the residuals* $R_i, i = 1, 2$ *are defined in* (2.13). *We identify the following:*

- $\mathcal{E}_0 = \sum_{i=1}^{2} (\phi_{i,0}, u_{i,0} - \pi u_{i,0})$ *as the initial error,*
- $\mathcal{E}_J = -\sum_{i=1}^{2} \sum_{n=1}^{N} (\phi_{i,n-1}, [u_i^h]_{n-1})$ *as the error due to the discontinuous approximation in time,*
- $\mathcal{E}_\Gamma = \sum_{n=1}^{N} \int_{I_n} < \mu, u_1^h - u_2^h > \, \mathrm{d}t$ *as the interface error,*
- $\mathcal{E}_\Omega = \sum_{i=1}^{2} \sum_{n=1}^{N} \int_{I_n} (R_i, \phi_i) \, \mathrm{d}t$ *as the domain error,*

and write

$$\mathcal{E} = \mathcal{E}_0 + \mathcal{E}_J + \mathcal{E}_\Gamma + \mathcal{E}_\Omega. \tag{3.7}$$

Proof. We use the errors e_1, e_2, and e_λ as test functions in the weak formulation of the adjoint problem (3.3) and (3.4), yielding

$$\int_0^T \left\{ \mp < \mu, u_i - u_i^h > - \left(\frac{\partial \phi_i}{\partial t}, u_i - u_i^h \right) + a_i(\phi_i, u_i - u_i^h) \right\} \, \mathrm{d}t = \int_0^T (\psi_i, e_i) \, \mathrm{d}t, \quad i = 1, 2,$$

$$\int_0^T \left\{ - < \lambda, \phi_1 - \phi_2 > + < \lambda^h, \phi_1 - \phi_2 > \right\} \, \mathrm{d}t = - \int_0^T < e_\lambda, \psi > \, \mathrm{d}t.$$

Adding these equations together, integrating by parts in time, and recalling the residual definition (2.13) and the piecewise constant dependence of the finite-element solution in time, we obtain

$$\mathcal{E} = \int_0^T \left\{ - < \mu, u_1 - u_2 > + < \mu, u_1^h - u_2^h > \right\} \, \mathrm{d}t - \sum_{i=1}^{2} \sum_{n=1}^{N} (\phi_i, u_i - u_i^h) \Big|_{t_{n-1}^+}^{t_n^-} \, \mathrm{d}t$$
$$+ \sum_{i=1}^{2} \int_0^T \left\{ \mp < \lambda, \phi_i > + \left(\frac{\partial u_i}{\partial t}, \phi_i \right) + a_i(u_i, \phi_i) + (R_i, \phi_i) - (f_i, \phi_i) \right\} \, \mathrm{d}t.$$

We can also use ϕ_1, ϕ_2 and μ as test functions in the weak formulation of the original problem (2.7) and (2.8), resulting in

$$\int_0^T \left\{ \mp < \lambda, \phi_i > -(f_i, \phi_i) + \left(\frac{\partial u_i}{\partial t}, \phi_i \right) + a_i(u_i, \phi_i) \right\} \, \mathrm{d}t = 0, \quad i = 1, 2,$$
$$- \int_0^T < \mu, u_1 - u_2 > \, \mathrm{d}t = 0.$$

Subtracting both expressions from the above formula for $\mathcal{E}$,

$$\mathcal{E} = \sum_{i=1}^{2} \sum_{n=1}^{N} \left\{ - \left(\phi_i, u_i - u_i^h \right) \Big|_{t_{n-1}^+}^{t_n^-} + \int_{I_n} \left\{ \pm < \mu, u_i^h > + (R_i, \phi_i) \right\} \, \mathrm{d}t \right\}. \tag{3.8}$$

We can rewrite the term due to jumps in the solution, assuming the exact solutions to the original and to the adjoint problems are continuous in time (within their respective subdomains), and using the initial and final conditions (2.2) and (3.5). Noting that

$$\sum_{n=1}^{N} \left(\phi_i, u_i - u_i^h \right) \Big|_{t_{n-1}^+}^{t_n^-} = -(\phi_{i,0}, u_{i,0}) - \sum_{n=1}^{N} \left(\phi_i, u_i^h \right) \Big|_{t_{n-1}^+}^{t_n^-},$$

the error measure can be written as

$$\mathcal{E} = \sum_{i=1}^{2} \left\{ (\phi_{i,0}, u_{i,0}) + \sum_{n=1}^{N} \left(\phi_i, u_i^h \right) \Big|_{t_{n-1}^+}^{t_n^-} + \sum_{n=1}^{N} \int_{I_n} \left\{ \pm < \mu, u_i^h > + (R_i, \phi_i) \right\} \, \mathrm{d}t \right\}.$$

Using the initial conditions $u_{i,0+}^h = \pi u_{i,0}$ and $\phi_{i,N} = 0$ to rearrange the first two terms we obtain the representation formula (3.6),

$$\mathcal{E} = \sum_{i=1}^{2} \left\{ (\phi_{i,0}, u_{i,0} - \pi u_{i,0}) - \sum_{n=1}^{N} (\phi_{i,n-1}, [u_i^h]_{n-1}) \right.$$
$$\left. + \sum_{n=1}^{N} \int_{I_n} \left\{ \pm < \mu, u_i^h > + (R_i, \phi_i) \right\} \, \mathrm{d}t \right\}. \qquad \square$$

Remark 1. Upon appropriate simplification, error representation formulas for a system comprising two coupled elliptic problems and for a system comprising a parabolic problem coupled to an elliptic problem, follow immediately from the above result.

We now consider corrections to the error representation formula due to errors on the boundary and error in the adjoint solution.

3.1. The effect of discretization error on the boundary. The proof of Theorem 3.1 utilized errors e_1 and e_2 as test functions in the adjoint problem. This is permissible only if the boundary conditions lie in the appropriate finite element spaces, i.e., if $u_i^D \in X_{i,D}^h, i = 1, 2$. In particular, the proof of Theorem 3.1 assumes that u_i^D is piecewise-constant in time.

In order to account for the circumstances when $u_i^D \notin X_{i,D}^h$, $i = 1, 2$, we introduce functions $e_i^D = u_i^D - \pi^h \theta u_i^D$ on Γ_i^D, $i = 1, 2$ for all $t \in I$. We extend this function to the whole domain $\Omega_1 \cup \Omega_2$ by setting it to zero at all mesh points other than those

on the Dirichlet boundaries, and allowing it to be piecewise linear in space. Then we can write

$$\int_0^T (\psi_i, e_i)\ \mathrm{d}t = \int_0^T (\psi_i, e_i - e_i^D)\ \mathrm{d}t + \int_0^T (\psi_i, e_i^D)\ \mathrm{d}t.$$

Now, $e_i - e_i^D$ is a suitable test function for the adjoint. Substituting for the first term on the right-hand side from (3.3),

$$\int_0^T (\psi_i, e_i)\ \mathrm{d}t = \int_0^T \left\{ \mp < \mu, e_i - e_i^D > - \left(\frac{\partial \phi_i}{\partial t}, e_i - e_i^D \right) + a_i(\phi_i, e_i - e_i^D) \right\}\ \mathrm{d}t + \int_0^T (\psi_i, e_i^D)\ \mathrm{d}t.$$

Proceeding as before, we define

$$\mathcal{E}_D = \sum_{i=1}^{2} \sum_{n=1}^{N} \int_{I_n} \left\{ \pm < \mu, e_i^D > + \left(\frac{\partial \phi_i}{\partial t}, e_i^D \right) - a_i(\phi_i, e_i^D) + (\psi_i, e_i^D) \right\}\ \mathrm{d}t, \tag{3.9}$$

and arrive at the full error representation

$$\mathcal{E} = \mathcal{E}_0 + \mathcal{E}_\Gamma + \mathcal{E}_J + \mathcal{E}_\Omega + \mathcal{E}_D, \tag{3.10}$$

where $\mathcal{E}_0,\ \mathcal{E}_\Gamma,\ \mathcal{E}_J,\ \mathcal{E}_\Omega$ are as defined in Theorem 3.1.

Remark 2. In a realistic case, a Dirichlet boundary condition is unlikely to be given in functional form, meaning it will automatically reside in the finite element space. Unless stated explicitly, we do not include this error component in the calculations below.

3.2. The effect of adjoint approximation. The effect of adjoint approximation has previously been considered by [10, 32, 37], amongst others. Let the adjoint finite element spaces $\hat{X}_1$, $\hat{X}_2$, and $\hat{Y}$ be such that $X_i^h \subset \hat{X}_i \subset X_i$ and $Y^h \subset \hat{Y} \subset Y$, and let $\hat{X}_{i,0} = \hat{X}_i \cap X_{i,0}$, $i = 1, 2$. Thus we solve the following: *Find* $(\phi_1^h, \phi_2^h, \mu^h) \in \hat{X}_{1,0} \times \hat{X}_{2,0} \times \hat{Y}$ *such that*

$$\sum_{n=1}^{N} \left(-([\phi_i^h]_n, v_{i,n-}^h) + \int_{I_n} \left\{ \mp < \mu^h, v_i^h > - \left(\frac{\partial \phi_i^h}{\partial t}, v_i^h \right) + a_i(\phi_i^h, v_i^h) \right\}\ \mathrm{d}t \right) = \sum_{n=1}^{N} \int_{I_n} (\psi_i, v_i^h)\ \mathrm{d}t \quad \forall v_i^h \in \hat{X}_{i,0}, \quad i = 1, 2, \tag{3.11}$$

$$\sum_{n=1}^{N} \int_{I_n} < \rho^h, \phi_1^h - \phi_2^h >\ \mathrm{d}t = \sum_{n=1}^{N} \int_{I_n} < \rho^h, \psi >\ \mathrm{d}t \quad \forall \rho^h \in \hat{Y}, \tag{3.12}$$

$$\phi_i^h(x, T) = 0 \quad \forall x \in \Omega_i, \quad i = 1, 2. \tag{3.13}$$

Note that the partition of the time interval I remains the same. A finer partition will introduce additional jump terms which we choose to avoid for ease of exposition. In practice, we employ dG(1) in time (discontinuous piecewise-linear functions), and cG(1) in space (continuous piecewise-linear functions) on a finer mesh than that used for the original finite element method.

THEOREM 3.2. *Let $(u_1^h, u_2^h, \lambda^h)$ be the finite element solution of (2.10)–(2.12), and let $(\phi_1^h, \phi_2^h, \mu^h)$ be the finite element solution of (3.11)–(3.13). Then the error in the quantity of interest defined by (3.6) can be represented as a sum of the estimated error $\mathcal{E}_{est}$ and a remainder ϵ, i.e.,*

$$\mathcal{E} = \mathcal{E}_{est} + \epsilon, \tag{3.14}$$

where

$$\begin{aligned}\mathcal{E}_{est} = \sum_{i=1}^{2} \Bigg\{ &(\phi_{i,0+}^h, u_{i,0} - \pi^h u_{i,0}) - \sum_{n=1}^{N} \left(\phi_{i,(n-1)+}^h, \left[u_i^h\right]_{n-1}\right) \\ &+ \sum_{n=1}^{N} \int_{I_n} \left\{ \pm < \mu^h, u_i^h > + (R_i, \phi_i^h) \right\} \, \mathrm{d}t \Bigg\},\end{aligned} \tag{3.15}$$

$$\epsilon = \sum_{i=1}^{2} \left\{ (\phi_{i,0} - \phi_{i,0+}^h, u_{i,0}) + \sum_{n=1}^{N} \int_{I_n} (f_i, \phi_i - \phi_i^h) \, \mathrm{d}t \right\}. \tag{3.16}$$

Proof. Analogous to the proof of Theorem 3.1. ∎

The value of ϵ is not computable but can be bounded a priori if f_i are sufficiently regular. We provide numerical evidence in section 5 that ϵ can indeed be neglected provided the adjoint finite element solution is sufficiently accurate.

4. An adaptive strategy. Our goal is to use the error representation formula (3.6) in order to obtain a mesh which is well-suited for a given problem and which achieves a specified error tolerance in a given quantity of interest. We consider the projection of the adjoint solution onto the original finite element space $(\pi^h\theta\phi_1, \pi^h\theta\phi_2, \pi^h\theta\mu)$, which can be used as a test function in the original finite element problem (2.10)–(2.11), and so satisfies

$$\begin{aligned}&\sum_{i=1}^{2}\sum_{n=1}^{N} \left\{ \left(\pi^h\theta\phi_{i,(n-1)+}^h, \left[u_i^h\right]_{n-1}\right) - \int_{I_n} (R_i, \pi^h\theta\phi_i^h) \, \mathrm{d}t \right\} = 0, \\ &-\sum_{n=1}^{N} \int_{I_n} < \pi^h\theta\mu^h, u_1^h - u_2^h > \, \mathrm{d}t = 0.\end{aligned}$$

Adding these equations together, we have

$$\sum_{i=1}^{2}\sum_{n=1}^{N} \left\{ (\pi^h\theta\phi_{i,(n-1)+}^h, \left[u_i^h\right]_{n-1}) \mp \int_{I_n} < \pi^h\theta\mu^h, u_i > \, \mathrm{d}t - \int_{I_n} (R_i, \pi^h\theta\phi_i^h) \, \mathrm{d}t \right\} = 0.$$

Combining with the representation formula (3.15), and adding and subtracting the term

$$\sum_{i=1}^{2}\sum_{n=1}^{N} \left\{ (\theta\phi_{i,(n-1)+}^h, \left[u_i^h\right]_{n-1}) \mp < \theta\mu^h, u_i > - \int_{I_n} (R_i, \theta\phi_i^h) \right\},$$

yields

$$\mathcal{E}_{est} = \sum_{i=1}^{2} \Bigg\{ (\phi_{i,0+}^h, u_{i,0} - \pi^h u_{i,0}) - \sum_{n=1}^{N} \left(\phi_{i,(n-1)+}^h - \theta \phi_{i,(n-1)+}^h, \left[u_i^h \right]_{n-1} \right)$$
$$- \sum_{n=1}^{N} \left(\theta \phi_{i,(n-1)+}^h - \pi^h \theta \phi_{i,(n-1)+}^h, \left[u_i^h \right]_{n-1} \right) + \sum_{n=1}^{N} \int_{I_n} \pm < \mu^h - \theta \mu^h, u_i^h > \, \mathrm{d}t$$
$$+ \sum_{n=1}^{N} \int_{I_n} \left\{ \pm < \theta \mu^h - \pi^h \theta \mu^h, u_i^h > + (R_i, \phi_i^h - \theta \phi_i^h) + (R_i, \theta \phi_i^h - \pi^h \theta \phi_i^h) \right\} \, \mathrm{d}t \Bigg\}.$$

This form of the error measure allows us to distinguish between the effects of approximation in time and in space. We group all terms involving $\phi^h - \theta \phi^h$ to produce the temporal error, and all terms involving $\theta \phi^h - \pi^h \theta \phi^h$ to produce the spatial error, and write the total error as the sum of these two components. Clearly, the initial error is part of the spatial approximation error. We compute the contributions to the temporal error at each time step, and the contributions to the spatial error on each element Δ at each time step I_n, i.e.,

$$\mathcal{E}_{est} = \mathcal{E}_t + \mathcal{E}_x$$

with

$$\mathcal{E}_t = \sum_{n=1}^{N} \mathcal{E}_t^n = \sum_{n=1}^{N} \left(\sum_{i=1,2} \sum_{\Delta_i \in \tau_i} \mathcal{E}_t^{n,\Delta_i} + \sum_{\gamma \in \tau} \mathcal{E}_t^{n,\gamma} \right),$$
$$\mathcal{E}_x = \sum_{i=1,2} \sum_{\Delta_i \in \tau_i} \mathcal{E}_0^{\Delta_i} + \sum_{n=1}^{N} \left(\sum_{i=1,2} \sum_{\Delta_i \in \tau_i} \mathcal{E}_x^{n,\Delta_i} + \sum_{\gamma \in \tau} \mathcal{E}_x^{n,\gamma} \right),$$

$$\mathcal{E}_t^{n,\Delta_i} = - \left(\phi_{i,(n-1)+}^h - \theta \phi_{i,(n-1)+}^h, \left[u_i^h \right]_{n-1} \right)_{\Delta_i}$$
$$+ \int_{I_n} \left\{ (f_i, \phi_i^h - \theta \phi_i^h)_{\Delta_i} - \left(\frac{\partial u_i^h}{\partial t}, \phi_i^h - \theta \phi_i^h \right)_{\Delta_i} - a_i(u_i^h, \phi_i^h - \theta \phi_i^h)_{\Delta_i} \right\} \, \mathrm{d}t,$$
$$n = 1, \ldots, N, \; i = 1, 2,$$
$$\mathcal{E}_t^{n,\gamma} = \sum_{i=1,2} \int_{I_n} \left\{ \pm < \mu^h - \theta \mu^h, u_i^h >_\gamma \pm < \lambda^h, \phi_i^h - \theta \phi_i^h >_\gamma \right\} \, \mathrm{d}t, \quad n = 1, \ldots, N,$$

$$\mathcal{E}_0^{\Delta_i} = (\phi_{i,0+}^h, u_{i,0} - \pi^h u_{i,0})_{\Delta_i}, \quad i = 1, 2,$$
$$\mathcal{E}_x^{n,\Delta_i} = - \left(\theta \phi_{i,(n-1)+}^h - \pi^h \theta \phi_{i,(n-1)+}^h, \left[u_i^h \right]_{n-1} \right)_{\Delta_i}$$
$$+ \int_{I_n} \left\{ (f_i, \theta \phi_i^h - \pi^h \theta \phi_i^h)_{\Delta_i} - \left(\frac{\partial u_i^h}{\partial t}, \theta \phi_i^h - \pi^h \theta \phi_i^h \right)_{\Delta_i} - a_i(u_i^h, \theta \phi_i^h - \pi^h \theta \phi_i^h)_{\Delta_i} \right\} \mathrm{d}t,$$
$$n = 1, \ldots, N, \; i = 1, 2,$$
$$\mathcal{E}_x^{n,\gamma} = \sum_{i=1,2} \int_{I_n} \left\{ \pm < \theta \mu^h - \pi^h \theta \mu^h, u_i^h >_\gamma \pm < \lambda^h, \theta \phi_i^h - \pi^h \theta \phi_i^h >_\gamma \right\} \, \mathrm{d}t,$$
$$n = 1, \ldots, N,$$

where

$$(u,v)_{\Delta_i} = \int_{\Delta_i} uv \ \mathrm{d}x, \ a_i(u,v)_{\Delta_i} = \int_{\Delta_i} \nabla u \cdot \nabla v \ \mathrm{d}x, \ <\nu, v>_\gamma = \int_\gamma \nu v \ \mathrm{d}s, \quad i = 1, 2.$$

Given a global tolerance TOL, the total number of elements in the domain and on the interface M, and the number of time steps N, we compute the local tolerance $LTOL = 2\ TOL/(NM)$. A time step n is marked for refinement if $|\mathcal{E}_t^n| > M \cdot LTOL$, an element Δ_i at time step n is marked for refinement if $|\mathcal{E}_x^{n,\Delta_i}| > LTOL$, and an interface edge γ at time step n is marked for refinement if $|\mathcal{E}_x^{n,\gamma}| > LTOL$. If an interface edge is refined, then the neighboring domain elements are refined as well.

Constructing a solution on a different spatial mesh at every time step can become extremely costly. Moreover, projection introduces additional errors and any gains from nonuniform refinements can be lost in the process of repeated projections. To overcome this difficulty we employ one of the blockwise time refinement techniques introduced in [8]. We group time steps into blocks so that a single refined spatial mesh is used to compute solutions within each space-time block. We prescribe an upper bound on the number of refinements allowed in a block, $NMAX$, introducing an effective upper bound on the number of elements in the refined mesh, and hence a restriction on the memory used. Clearly TOL and $NMAX$ are related, and it is possible to construct situations in which the desired accuracy cannot be achieved with the prescribed maximum number of refinements. The severity of this issue will depend upon the accuracy desired.

We start from a single temporal block corresponding to the original mesh, including all time steps. Starting from $t = 0$ the required refinements are applied to the original mesh for consecutive time steps until a block is "full," i.e., the number of required refinements reaches $NMAX$. Then a new block is formed from the original mesh and the process is repeated starting from the following time step. For details of the method we refer to the original paper [8].

This algorithm can result in more than $NMAX$ refinements in a block, first, because a new block is created only after this upper limit is exceeded, and second, because the resulting triangulation is regularized, i.e., additional edges are introduced to remove hanging nodes. Depending on the refinement limits and the behavior of the solution, this strategy can result in anything from a single time block to a block every time step. The flexibility of the algorithm to automatically obtain reliable block mesh refinements, under constraints such as the user's available computational power, storage, and processing time, will be illustrated in the following section.

5. Numerical examples of the effectivity of the error estimate. We investigate the accuracy of the representation formula (3.10) in a variety of scenarios for which exact solutions are known, allowing an effectivity ratio of

$$\mathcal{R} = \frac{\mathcal{E}_{est}}{\mathcal{E}} \tag{5.1}$$

to be calculated. Since the refinements are based on the absolute values of local errors, we also consider the effect of summing the absolute value of error contributions. We define

$$\overline{\mathcal{E}} = \sum_{n=1}^{N} \int_{I_n} \left\{ \sum_{\gamma \in \tau} |< e_\lambda, \psi >_\gamma| + \sum_{\Delta_1 \in \tau_1} |(e_1, \psi_1)_{\Delta_1}| + \sum_{\Delta_2 \in \tau_2} |(e_2, \psi_2)_{\Delta_2}| \right\} \ \mathrm{d}t,$$

and $\overline{\mathcal{E}}_{est} = \overline{\mathcal{E}}_t + \overline{\mathcal{E}}_x$, where

$$\overline{\mathcal{E}}_t = \sum_{n=1}^{N} \left(\sum_{i=1,2} \sum_{\Delta_i \in \tau_i} \left| \mathcal{E}_t^{n,\Delta_i} \right| + \sum_{\gamma \in \tau} |\mathcal{E}_t^{n,\gamma}| \right),$$

$$\overline{\mathcal{E}}_x = \sum_{i=1,2} \sum_{\Delta_i \in \tau_i} \left| \mathcal{E}_0^{\Delta_i} \right| + \sum_{n=1}^{N} \left(\sum_{i=1,2} \sum_{\Delta_i \in \tau_i} \left| \mathcal{E}_x^{n,\Delta_i} \right| + \sum_{\gamma \in \tau} |\mathcal{E}_x^{n,\gamma}| \right).$$

The corresponding effectivity ratio is

$$\overline{\mathcal{R}} = \frac{\overline{\mathcal{E}}_{est}}{\overline{\mathcal{E}}}.$$

We begin by examining the "domain decomposition" scenario in which there is a single operator and a single solution within the entire domain which we choose to subdivide for computational purposes. We then consider problems in which distinct operators and/or distinct solutions pertain to the two subdomains, including the case in which an elliptic operator in one domain is coupled to a parabolic operator in the other domain. In this case the arguments described in section 3 must be suitably (though easily) modified. We also consider situations in which the discretizations do not conform along the interface, the situation arising in mortar finite element methods. In all cases, (3.10) provides an accurate estimate of the numerical error which improves as the adjoint solution is refined.

5.1. Single operator in Ω_1 and Ω_2. By setting $\mathcal{L}_1 = \mathcal{L}_2$ the interface conditions guarantee that the solution of the coupled problem (2.1)–(2.6) is the same as the problem in a single domain Ω,

$$\begin{aligned} \frac{\partial u}{\partial t} + \mathcal{L}u &= f && \text{in } \Omega \times (0,T], \\ u(x,y,0) &= u_0(x,y) && (x,y) \in \Omega, \\ u &= u^D && \text{on } \Gamma^D \times (0,T], \\ \frac{\partial u}{\partial n} &= 0 && \text{on } \Gamma^N \times (0,T], \end{aligned}$$

where $\Gamma^D \cup \Gamma^N = \partial\Omega$ and $\Gamma^D \cap \Gamma^N = \emptyset$. Here $\Omega := \{(x,y) \in (0,1)\times(0,2)\}$, $\Gamma^D := \{x \in \partial\Omega,\ y = 0,2\}$ and $\Gamma^N := \{x \in \partial\Omega,\ x = 0,1\}$. Further $\Omega_1 := \{(x,y) \in (0,1) \times (0,1)\}$ and $\Omega_2 := \{(x,y) \in (0,1) \times (1,2)\}$. We note that this scenario is similar to that arising in domain decomposition [34].

5.1.1. Domain error. We first consider the quantity of interest to be a function of solutions u_1 and u_2 only. In the following examples $\mathcal{L}u = -\Delta u$ and the right-hand sides, the initial and boundary conditions are obtained using the exact solution. The quantity of interest is a weighted average solution in the (space-time) domain, so that the adjoint solution can be obtained in closed form as $\phi = 0.5(T-t)y(2-y)$. The problem was solved with $N_t = 5$ time steps on $t \in (0,1]$ and for an original mesh containing $DOF = 78$ degrees of freedom. We consider five test problems with exact solutions:

$$\text{(i) } u = 0.5y(2-y), \quad \text{(ii) } u = 0.5ty(2-y), \quad \text{(iii) } u = t\sin(0.5\pi y),$$
$$\text{(iv) } u = y + t \qquad \text{(v) } u = y + \sin(t),$$

and report effectivity ratios in Table 5.1 for varying the spatial accuracy of the adjoint solution. In all problems the adjoint finite element solution was computed on a mesh obtained by refining the corresponding primal problem mesh $r = 1, 2$, or 3 times. In this way we satisfy the condition that the original and adjoint finite element spaces be nested, i.e., $X_i^h \subset \hat{X}_i$, $i = 1, 2$, and $Y^h \subset \hat{Y}$.

TABLE 5.1

Subsection 5.1. *Effectivity ratios* $\mathcal{R}$ *and* $\overline{\mathcal{R}}$*, for model problems* (i)–(v) *varying the spatial accuracy of the adjoint solution. The value of* r *corresponds to the number of uniform spatial refinements used to obtain the adjoint mesh from the adapted mesh on which the solution is computed. The problem was solved with* $N_t = 5$ *time steps, final time* $T = 1$*, and the original mesh of* $DOF = 78$ *degrees of freedom.*

r	$\mathcal{R}$				
	(i)	(ii)	(iii)	(iv)	(v)
1	0.8499	1.0151	1.0129	1.0000	1.0000
2	0.9625	1.0038	1.0033	1.0000	1.0000
3	0.9906	1.0009	1.0009	1.0000	1.0000
r	$\overline{\mathcal{R}}$				
	(i)	(ii)	(iii)	(iv)	(v)
1	2.6508	1.2455	1.2431	1.1444	1.4021
2	3.2115	1.2911	1.2902	1.1803	1.4516
3	3.3514	1.3024	1.3019	1.1893	1.4640

As expected, the calculated effectivity ratios $\mathcal{R}$ for problems (i)–(iii) approach one as the accuracy of the adjoint solution increases. The exact adjoint solution $\phi = 0.5(T - t)y(2 - y)$ is linear in time and quadratic in space, hence the finite element method used (dG(1) in time, cG(1) in space) can capture temporal variation exactly, while spatial refinements of the adjoint mesh reduce the error in the adjoint solution.

In problems (iv) and (v), the spatial errors in the adjoint finite element solution are symmetric about $y = 1$ leading to cancelation in the term $(f, \phi - \phi^h)$ in (3.16). Problems (iv) and (v) were chosen so that the boundary conditions do not lie in the finite element space (are not piecewise constant in time). When the error is calculated according to the original formula (3.6) (omitting the boundary error), the effectivity ratio in both problems $\mathcal{R} \approx 0.4$ independently of the accuracy of the mesh on which the adjoint problem is solved. Despite the fact that the Dirichlet boundary error $\mathcal{E}_D$ is small, it is significant in relation to the overall error and cannot be ignored.

If we choose to sum the absolute values of the error contributions on each element, eliminating the possibility for cancelation of error between elements, we compute the effectivity ratios $\overline{\mathcal{R}}$ shown in Table 5.1. These ratios are not as close to 1 as $\mathcal{R}$, and moreover, do not converge to one as the adjoint solution converges.

5.1.2. Interfacial error. To estimate interfacial errors we consider the test problem with the exact solution (vi) $u = t\sin(\pi y)$. In order to obtain an adjoint solution in closed form, specifically $\phi_1 = 0.5(T - t)y$ and $\phi_2 = 0.5(T - t)(y - 2)$, the weighting functions for the quantity of interest are chosen to be $\psi_1 = 0.5y$, $\psi_2 = (0.5y - 1)$ and $\psi = T - t$. Note that the adjoint solution satisfies zero Dirichlet conditions at $y = 0, 2$, zero Neumann conditions at $x = 0, 1$, and zero conditions at $t = T$. Note too, that these adjoint weights do not correspond to pure interface error.

However, since

$$\frac{|\mathcal{E}_\Gamma|}{|\mathcal{E}|} = \frac{\left|\int_0^T < \psi, e_\lambda > \ \mathrm{d}t\right|}{\left|\int_0^T \{- < \psi, e_\lambda > + (\psi_1, e_1) + (\psi_2, e_2)\} \ \mathrm{d}t\right|} = 0.7669,$$

the interface error is a significant part of the total error. We report effectivity ratios for mixed domain and interface error in columns two and three of Table 5.2. The adjoint solution is captured exactly by the finite element method, and the effectivity ratios are therefore equal to one.

TABLE 5.2

Subsection 5.1.2. *Effectivity ratios* $\mathcal{R}$ *and* $\overline{\mathcal{R}}$*, varying the spatial accuracy of the adjoint solution. The value of* r *corresponds to the number of uniform spatial refinements used to obtain the adjoint mesh from the adapted mesh on which the solution is computed. The problem was solved with* $N_t = 5$ *time steps, final time* $T = 1$*, and the original mesh of* $DOF = 253$ *degrees of freedom for the conforming (conf) meshes and* $DOF = 393$ *for the nonconforming (nonconf) meshes.*

r	(vi) Mixed error		(vi) Interface error	
	(conf)	(nonconf)	(conf)	(nonconf)
	$\mathcal{R}$			
1	1.0000	1.0000	0.9925	0.9946
2	1.0000	1.0000	0.9982	0.9987
3	1.0000	1.0000	0.9996	0.9997
r	$\overline{\mathcal{R}}$			
1	0.9647	0.9761	1.1238	1.1075
2	0.9647	0.9761	1.1623	1.1397
3	0.9647	0.9761	1.1720	1.1478

In order to calculate purely interfacial error, we set $\psi_1 = \psi_2 = 0$ and $\psi = T - t$ (to satisfy the condition at $t = T$). We report effectivity ratios for the interfacial error in columns four and five of Table 5.2.

We consider both triangulations in Ω_1 and Ω_2 that conform on the interface (see Figure 5.1(a)) and those that do not (see Figure 5.1(b)). Conforming discretizations have 121 degrees of freedom in each domain and 11 on the interface. Nonconforming discretizations have 121 degrees of freedom in Ω_1, 256 in Ω_2, and 16 on Γ. As seen in Table 5.2, the calculated effectivity ratios $\mathcal{R}$ for both conforming and nonconforming cases converge to one as the adjoint mesh is refined.

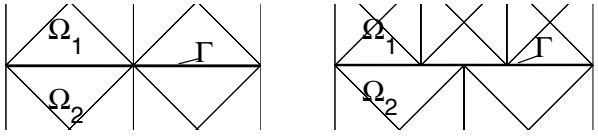

(a) Conforming meshes (b) Nonconforming meshes

FIG. 5.1. *Conforming versus nonconforming meshes in domains* Ω_1 *and* Ω_2 *with a common interface* Γ.

Summing the absolute values of the error contributions on each element and thus eliminating the possibility for cancelation of error between elements, we compute the effectivity ratios $\overline{\mathcal{R}}$ shown in Table 5.2.

5.2. Distinct problems in Ω_1 and Ω_2. We now consider situations where there are distinct problems in the two domains Ω_1 and Ω_2. Problem (vii) is representative of the canonical mortar element situation with a single operator and different

solutions in each subdomain. Problem (viii) addresses the situation in which there are different operators in each subdomain. Problem (ix) is relevant to many fluid-solid interaction problems in which an elliptic problem has a time-dependent solution since it is coupled to a time-dependent (parabolic) problem.

(vii) $\mathcal{L}_1 u = \mathcal{L}_2 u = -\Delta u$, with exact solutions $u_1 = 0.5ty(2-y)$ and $u_2 = -0.5t\cos(0.5\pi(3-y))$.

(viii) $\mathcal{L}_1 u = -\Delta u$ and $\mathcal{L}_2 u = -0.1\Delta u + u$, with exact solutions $u_1 = t\sin(\pi y)$ and $u_2 = 10t\sin(\pi y)$.

(ix) Elliptic-parabolic coupling,

$$-\Delta u_1 = f_1 \text{ in } \Omega_1,$$
$$\frac{\partial u_2}{\partial t} - \Delta u_2 = f_2 \text{ in } \Omega_2,$$

with the usual initial, boundary, and coupling conditions, and the right-hand sides such that $u_1 = u_2 = 0.5ty(2-y)$.

The quantity of interest was once again chosen such that $\phi = 0.5(T-t)y(2-y)$. All problems were solved on $t \in (0,1]$ using $N_t = 5$ time steps. We report our results in Table 5.3. Spatial errors dominated in all three cases, and the effectivity ratio converged to one with spatial refinements for both conforming and nonconforming meshes in Ω_1 and Ω_2.

TABLE 5.3

Subsection 5.2. *Effectivity ratios* $\mathcal{R}$ *and* $\overline{\mathcal{R}}$*, for model problems* (vii)–(ix) *varying the spatial accuracy of the adjoint solution. The value of* r *corresponds to the number of uniform spatial refinements used to obtain the adjoint mesh from the adapted mesh on which the solution is computed. The problem was solved with* $N_t = 5$ *time steps, final time* $T = 1$*, and the original mesh of* $DOF = 78$ *degrees of freedom for the conforming (conf) meshes and* $DOF = 108$ *for the nonconforming (nonconf) meshes.*

r	(vii)		(viii)		(ix)	
	conf	nonconf	conf	nonconf	conf	nonconf
	$\mathcal{R}$					
1	1.0140	1.0091	1.0056	0.9974	1.0253	1.0137
2	1.0035	1.0023	1.0023	0.9993	1.0063	1.0034
3	1.0009	1.0006	1.0015	0.9997	1.0016	1.0008
	$\overline{\mathcal{R}}$					
1	1.2443	1.2028	1.3405	1.3058	1.4468	1.3610
2	1.2907	1.2422	1.3614	1.3246	1.5337	1.4342
3	1.3022	1.2521	1.3666	1.3293	1.5554	1.4524

Once again summing the absolute values of the error contributions on each element and eliminating the possibility for cancelation of error between elements, we compute the effectivity ratios $\overline{\mathcal{R}}$ shown in Table 5.3.

6. Numerical examples of adaptive mesh refinement. We apply the adaptive strategy described in section 4 to a sequence of problems and discuss the results obtained. We first consider situations in which a single domain with a single operator and solution is divided, perhaps for computational reasons. We then consider the effect of different operators. As before, $\Omega_1 = (0,1)\times(0,1)$ and $\Omega_2 = (0,1)\times(1,2)$. For a given mesh (whether uniform, or locally refined) the adjoint problem is solved on the same mesh refined once uniformly.

6.1. Single elliptic operator in Ω_1 and Ω_2 with different order finite elements. In order to highlight the effect of different order approximations on mesh

refinement we solve an *elliptic* problem using quadratic finite elements in Ω_1 and linear finite elements in Ω_2. We consider a (QoI) in the whole domain by setting $\psi_1 = 1$, $\psi_2 = -1$ and $\psi = 0$ and choosing f and boundary conditions such that $u_1 = u_2 = \sin(\pi x)\sin(\pi y)$, and a (QoI) on the interface by setting $\psi_1 = \psi_2 = 0$ and $\psi = \cos(\pi x)$ and choosing f and boundary conditions such that $u_1 = u_2 = \cos(\pi x)\sin(\pi y)$. The initial meshes in Ω_1 and Ω_2 are identical. The global tolerance was set to $TOL = 0.01$ for the quantity of interest in the domain, and $TOL = 0.06$ for the quantity of interest on the interface.

Since higher order elements are utilized in Ω_1, we expect the error there to be significantly lower than in Ω_2, and for the meshes to be refined accordingly. Indeed, in both problems the only refinements in Ω_1 occur near Γ to ensure compatibility between the meshes in the domains and on the interface. By contrast, the number of degrees of freedom in Ω_2 increased by a factor of ~ 10. The refined meshes are shown in Figure 6.1(a), and the errors and corresponding effectivity ratios are shown in Table 6.1. Note that in the case of interface errors the mesh is not refined around $x = 0.5$ where the weighting of the quantity of interest is zero.

We define the standard L_2-norm errors of the solution in the domain and on the interface as

$$e_\Omega = \left(\sum_{i=1}^{2} \int_0^T \int_{\Omega_i} \left(u_i - u_i^h\right)^2 \, \mathrm{d}x \, \mathrm{d}t \right)^{1/2} \quad \text{and} \quad e_\Gamma = \left(\int_0^T \int_{\Gamma} \left(\lambda - \lambda^h\right)^2 \, \mathrm{d}x \, \mathrm{d}t \right)^{1/2}.$$

The computed errors, shown in Table 6.1, decrease as the mesh is refined, although not necessarily as dramatically as the errors in the quantity of interest.

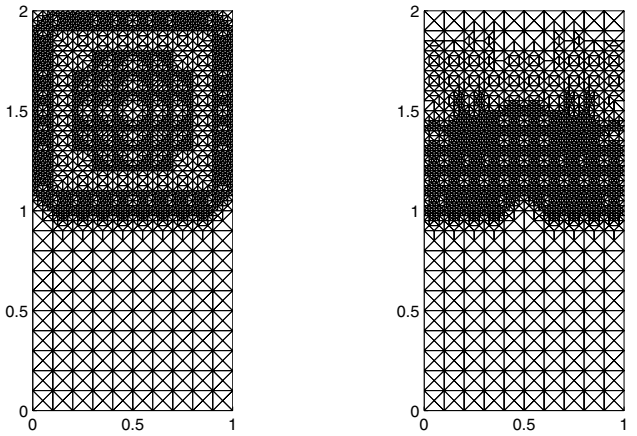

(a) (b)

FIG. 6.1. *Subsection* 6.1. *Meshes after space refinement using quadratic finite-elements in* Ω_1 *and linear finite-elements in* Ω_2. (a) *Refinement based on error in the domain.* (b) *Refinement based on error on the interface.*

6.2. Single parabolic operator in Ω_1 and Ω_2. Next, we consider a parabolic problem with $\mathcal{L}_1 u = \mathcal{L}_2 u = -\Delta u$, and return to using linear elements in both domains. The right-hand sides and the initial and Dirichlet boundary conditions were chosen so that

$$u = \exp(-100(x - 0.5 - 0.25\sin(\pi t))^2 - 100(y - 1 - 0.5\cos(\pi t))^2).$$

TABLE 6.1

Subsection 6.1. *Estimated total errors and effectivity ratios for both original and refined meshes using quadratic finite-elements in Ω_1 and linear finite-elements in Ω_2. DOF_1 and DOF_2 are the numbers of degrees of freedom in each sub-domain.*

	Average error in $\Omega_1 \cup \Omega_2$			
	$DOF_{1/2}$	$10^3\mathcal{E}_{est}$	$\mathcal{R}$	$10^3 e_\Omega$
Original	841/221	2.6808	0.9628	4.1934
Refined	1447/2265	0.4854	0.9659	0.7086
	Weighted average error on Γ			
Original	841/221	3.4658	0.9857	8.9262
Refined	1451/1837	0.0476	0.8387	1.1442

This solution is a Gaussian with a peak located at $(0.5, 1.5)$ at time $t = 0$, and moving clockwise along an elliptic trajectory inside $\Omega_1 \cup \Omega_2$. At the final time $T = 2$, the peak returns to its initial position after making one complete orbit. A snapshot view of the solution is presented in Figure 6.2(a). Unless stated otherwise, we began the adaptive procedure with a uniform mesh containing 453 degrees of freedom, and 200 equally distributed time steps.

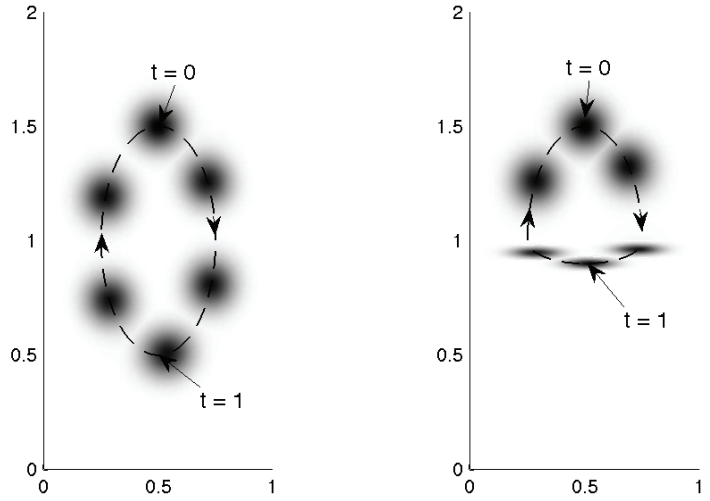

(a) $k_1 = k_2 = 1$ (b) $k_1 = 0.2,\ k_2 = 1$

FIG. 6.2. *Subsections* 6.2 *and* 6.3. *Cartoon of the solutions as a function of time.*

6.2.1. Adaptivity based on error in the domain only. First, we consider the quantity of interest representing the average in the whole domain, so that

$$\mathcal{E} = \int_0^T \left\{ \int_{\Omega_1} e_1 \, \mathrm{d}x + \int_{\Omega_2} e_2 \, \mathrm{d}x \right\} \, \mathrm{d}t,$$

i.e., $\psi_1 = \psi_2 = 1$ and $\psi = 0$. The global tolerance was set to $TOL = 0.01$. We allowed at most three refinements of an element, and at most six new time steps within an original time step. The maximum number of triangles marked for refinements in each temporal block was set at $NMAX = 400$. In practice more triangles were refined in

order to prevent hanging nodes or distorted elements. In all cases time steps were refined independently of the number of mesh blocks produced.

The time-space adaptive refinement strategy applied to the original uniform mesh produced six temporal blocks $I_1, \ldots, I_6$ shown in Figure 6.3. As expected, the spatial mesh refinements trace the movement of the Gaussian shaped "peak" of the solution in the domain. Away from the peak of the Gaussian, where the solution approaches a constant, the original mesh provides sufficiently good resolution and need not be refined.

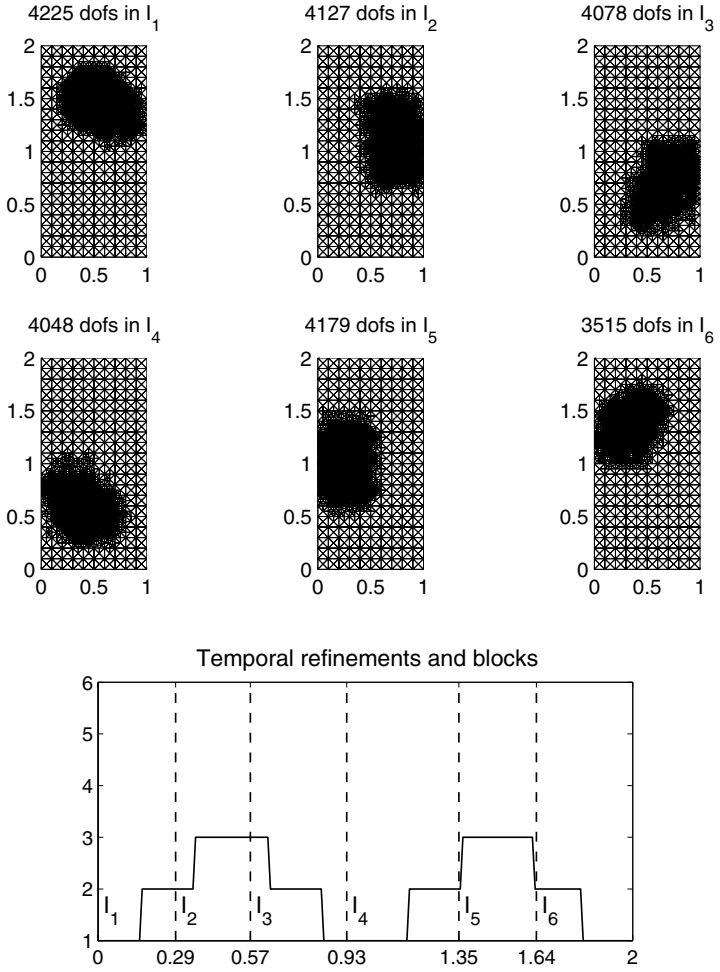

FIG. 6.3. *Subsection* 6.2.1. *Space/time blocks and temporal refinements produced for the quantity of interest equal to the average solution over the whole domain* $\Omega_1 \cup \Omega_2$ *given* $NMAX = 400$.

In Figure 6.3 we also show temporal refinements, namely how many time steps (between 1 and 6) the adaptive strategy produces for a single old time step. The observed temporal refinements are concentrated around $t = 0.5$ and $t = 1.5$, at which points of its elliptical orbit the peak is moving most rapidly. The estimated errors on the original and refined meshes are given in Table 6.2. We immediately observe the effect of error cancelation in the case of signed errors $\mathcal{E}$, they are at least one order

of magnitude lower than their absolute value counterparts $\overline{\mathcal{E}}$. In addition, the spatial component is dominant throughout for $\mathcal{E}$, while the temporal component becomes significant postrefinement for $\overline{\mathcal{E}}$. Note that since the refinement strategy relies on the absolute errors, temporal refinements are carried out even though $\mathcal{E}_t$ is very small. Overall, applying the method resulted in $\mathcal{E}$ decreasing by an order of magnitude, $\overline{\mathcal{E}}$ decreasing by a factor of 3, and the L_2-error e_Ω decreasing by a factor of 7.

TABLE 6.2

Subsection 6.2.1. *Estimated total errors $\mathcal{E}_{est}$ and $\overline{\mathcal{E}}_{est}$ for the quantity of interest equal to the average solution over the whole domain, the temporal and spatial components of the error $\mathcal{E}_t$ and $\mathcal{E}_x$, and the corresponding L_2-error e_Ω calculated on the original uniform mesh and on the refined mesh with $NMAX = 400$. DOF is the maximum number of degrees of freedom in a temporal block.*

Mesh (DOF)	$10^4\mathcal{E}_{est}$	$10^4\mathcal{E}_t$	$10^4\mathcal{E}_x$	$10^2\overline{\mathcal{E}}_{est}$	$10^2\overline{\mathcal{E}}_t$	$10^2\overline{\mathcal{E}}_x$	$10^2 e_\Omega$
Original (453)	−3.0997	−0.0049	−3.0948	1.7955	0.9589	0.8367	3.5884
Refined (4225)	−0.1448	−0.0033	−0.1415	0.6196	0.5446	0.0750	0.5238

In the method proposed in section 4 we apply all mesh refinements at once, allowing each element and time step to be subdivided multiple times. An alternative would be to apply refinements iteratively, and only allow elements and time steps to be refined once per iteration. The latter approach involves recalculating both the primal and the dual solutions, as well as the error estimate, after each refinement. The resulting errors and meshes are therefore more fine-tuned. However, the overhead computational costs of solving both the primal and the dual problems repeatedly on increasingly finer meshes, and computing the error estimates, are very substantial.

In order to compare the single-step and iterative strategies, we solve the problem with the quantity of interest equal to the average solution in the domain over all time. We start with a uniform mesh of 128 degrees of freedom and 100 uniform time steps, and set the global tolerance to 0.005. The maximum number of refinements in a block $NMAX$ must vary depending on the maximum number of refinements allowed in an element, and therefore has to be different for the two strategies if our goal is to produce the same number of temporal blocks for comparison. We set $NMAX = 210$ for the single-step method, and $NMAX = 100$ for the iterative method. The resulting spatial meshes are presented in Figure 6.4, and the errors in Table 6.3. In the single-step strategy we allow each element and time step to be subdivided at most three times, i.e., into eight elements/time steps, respectively. This is equivalent to allowing a single refinement of an element/time step per iteration in the iterative strategy.

The difference in the resulting meshes (at most 2164 degrees of freedom in the single-step process, and at most 1707 in the iterative process) is mainly due to the fact that multiple refinements of the original coarse mesh require more additional elements to avoid hanging nodes or distorted elements. The final number of time steps is higher in the iterative method: 673 compared to 634. There is no significant difference in the final errors, so the computational cost can be considered the most important factor in the choice of the method. We therefore proceed with the single-step method.

We also note that in contrast to the locally refined meshes, which in the above problem contain at most 2164 degrees of freedom in a block for $NMAX = 210$, a thrice uniformly refined mesh contains 6603 degrees of freedom. Similarly, the total number of time steps produced by the adaptive strategy is 634 compared to 800 in the uniformly refined case. The error estimates computed on uniformly refined meshes are shown in Table 6.4.

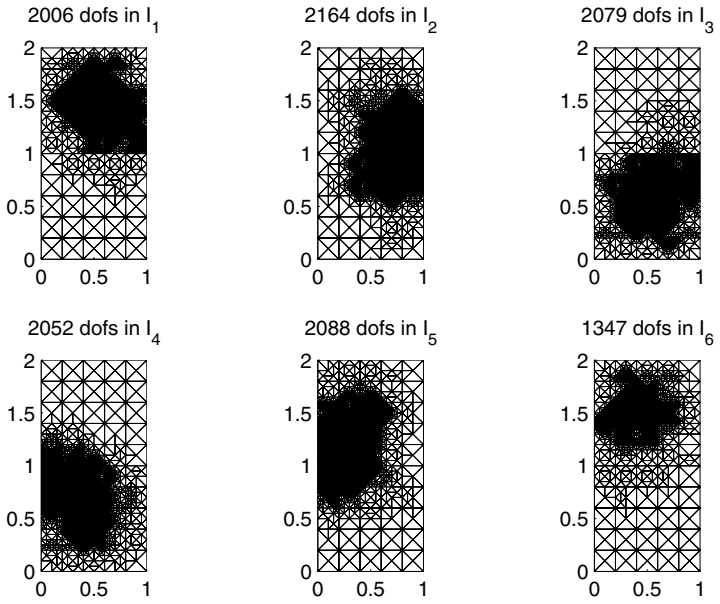

(a) Single-step refinement strategy, $NMAX = 210$

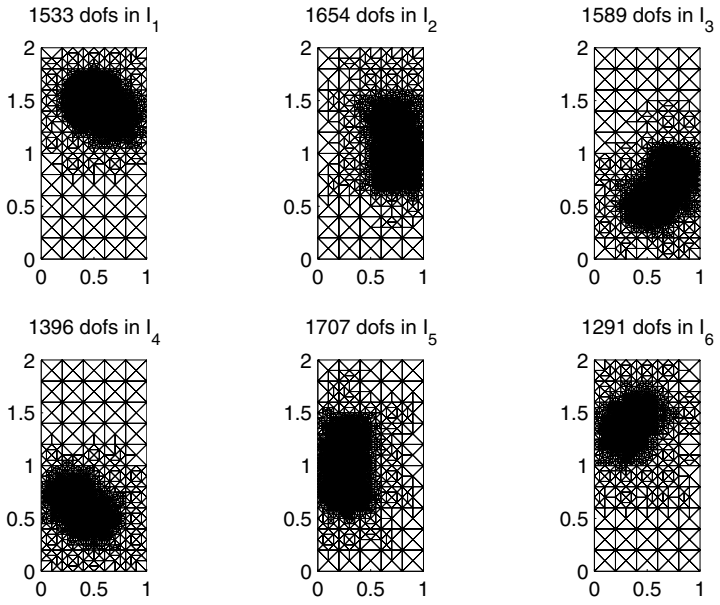

(b) Iterative refinement strategy, $NMAX = 100$

FIG. 6.4. *Space/time blocks produced for the quantity of interest equal to the average solution over the whole domain* $\Omega_1 \cup \Omega_2$.

TABLE 6.3

Estimated total errors $\mathcal{E}_{est}$ and $\overline{\mathcal{E}}_{est}$ computed for a quantity of interest equal to the average over the whole domain using the single-step (multiple refinements at once) and the iterative strategies (single refinement per iteration). DOF is the maximum number of degrees of freedom in a temporal block.

Mesh (DOF)	$10^3\mathcal{E}_{est}$	$10^3\mathcal{E}_t$	$10^3\mathcal{E}_x$	$10^2\overline{\mathcal{E}}_{est}$	$10^2\overline{\mathcal{E}}_t$	$10^2\overline{\mathcal{E}}_x$	$10^1 e_\Omega$
Single-step strategy							
1 (128)	−1.0833	−0.0202	−1.0631	4.2741	1.6699	2.6042	1.0624
2 (2164)	−0.0105	0.0004	−0.0109	0.4610	0.3106	0.1504	0.0403
Iterative strategy							
1 (128)	−1.0833	−0.0202	−1.0631	4.2741	1.6699	2.6042	1.0624
2 (329)	−0.1159	−0.0020	−0.1139	1.8438	0.9554	0.8883	0.3698
3 (696)	−0.0375	0.0001	−0.0376	0.8368	0.4981	0.3387	0.1127
4 (1707)	−0.0136	−0.0001	−0.0135	0.4522	0.3000	0.1522	0.0394

TABLE 6.4

Estimated total errors $\mathcal{E}_{est}$ and $\overline{\mathcal{E}}_{est}$ computed for a quantity of interest equal to the average over the whole domain on uniformly refined meshes. DOF is the total number of degrees of freedom in a mesh, N_t is the total number of time steps.

Mesh (DOF/N_t)	$10^3\mathcal{E}_{est}$	$10^2\overline{\mathcal{E}}_{est}$
1 (128/100)	−1.0833	4.2741
2 (453/200)	−0.1181	1.8619
3 (1703/400)	−0.0547	0.8346
4 (6603/800)	−0.0081	0.4021

The absolute error $\overline{\mathcal{E}}_{est}$ only reaches the tolerance $TOL = 0.005$ on mesh 4, i.e., after three uniform refinements of the original mesh. The reason for the rapid decay of the actual error $\mathcal{E}_{est}$ with uniform refinement is the cancelation of errors due to the symmetry of the problem. This cannot be guaranteed, and will not necessarily occur in other problems.

6.2.2. Adaptivity based on error along the interface. The weighted averaged error along the interface is calculated as

$$\mathcal{E} = \int_0^T \int_\Gamma \psi e_\lambda \, \mathrm{d}s \, \mathrm{d}t,$$

which corresponds to the adjoint right-hand sides $\psi_1 = \psi_2 = 0$ and $\psi \neq 0$. The adjoint solution has a jump across the interface $\phi_1 - \phi_2 = \psi$ on Γ. In order for this to conform with the Dirichlet boundary conditions for $\phi_1 = \phi_2 = 0$, we need to have $\psi = 0$ at $(0, 1)$ and $(1, 1)$. We also require $\phi_1 - \phi_2 = 0$ at $t = T$. To satisfy these conditions we chose $\psi = (T - t)\sin(\pi x)$. The global tolerance was set to $TOL = 0.05$. In this example we set block capacity to $NMAX = 550$ elements, and obtained three temporal blocks with at most 6027 degrees of freedom, as shown in Figure 6.5. Even though the peak of the Gaussian is almost fully contained in Ω_1 and does not intersect Γ in the second block $t \in I_2 = (0.5, 1.2]$, there is significant refinement of the mesh around the interface in Ω_2, where the quantity of interest is supported. The last block $t \in I_3 = (1.2, 2]$ is less refined around the point $(0.5, 1.5)$ than the first block. The reason for this is that while the accuracy of the solution for $t < 1.5$ directly affects the accuracy of the solution on the interface through which the Gaussian passes at $t = 0.5$ and $t = 1.5$, the accuracy with which the Gaussian is resolved for $t > 1.5$ will have little effect on the interface values. Moreover, the weighting of the interface error decreases linearly with $T - t$, and therefore it is more important to capture the

solution at the beginning of $(0, T]$ as compared to the end. For the same reason the temporal refinements shown in Figure 6.5, concentrated near $t = 0.5$ and $t = 1.5$, were much more pronounced in the first two blocks than in the third.

The error estimates are given in Table 6.5. Both $\mathcal{E}_{est}$ and $\overline{\mathcal{E}}_{est}$ were reduced by approximately an order of magnitude. Note that while the temporal error $\mathcal{E}_t$ was higher on the refined mesh than on the original mesh (due to lack of cancelation), its absolute value counterpart $\overline{\mathcal{E}}_t$, which drives temporal refinements, was reduced by an order of magnitude.

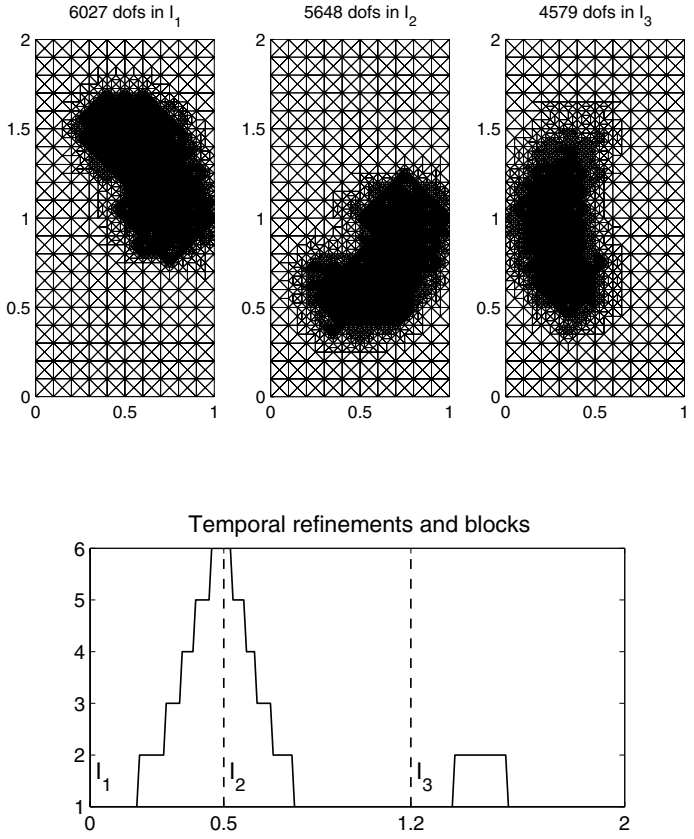

FIG. 6.5. *Subsection* 6.2.2. *Space/time blocks and temporal refinements obtained for a quantity of interest equal to the weighted average solution on the interface* Γ *given* $NMAX = 550$.

TABLE 6.5

Subsection 6.2.2. *Estimated total errors* $\mathcal{E}_{est}$ *and* $\overline{\mathcal{E}}_{est}$ *for the quantity of interest defined on the interface, the temporal and spatial components of the error* $\mathcal{E}_t$ *and* $\mathcal{E}_x$*, and the corresponding* L_2*-error* e_Γ *calculated on the original uniform mesh and on the mesh obtained after a space-time refinement with* $NMAX = 550$. DOF *is the maximum number of degrees of freedom in a temporal block.*

Mesh (DOF)	$10^4\mathcal{E}_{est}$	$10^4\mathcal{E}_t$	$10^4\mathcal{E}_x$	$10^2\overline{\mathcal{E}}_{est}$	$10^2\overline{\mathcal{E}}_t$	$10^2\overline{\mathcal{E}}_x$	$10^2 e_\Gamma$
Original (453)	−3.6602	−0.0013	−3.6615	7.3610	4.1043	3.2566	2.1835
Refined (6027)	−0.1448	−0.0033	−0.1415	0.6196	0.5446	0.0750	0.5238

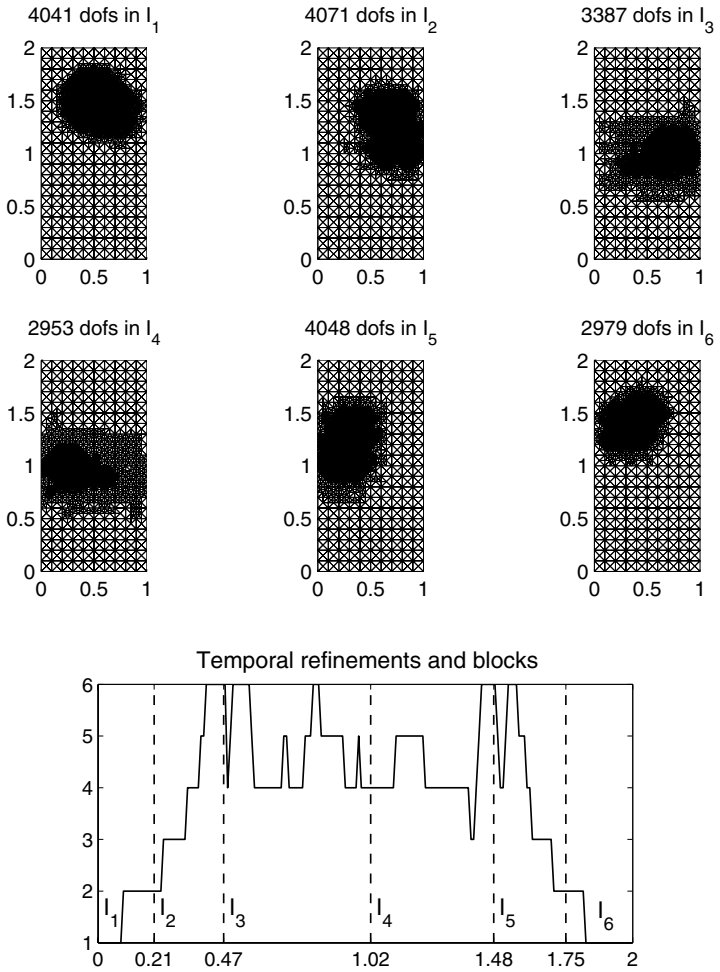

FIG. 6.6. *Subsection* 6.3(a). *Space/time blocks and temporal refinements produced for the quantity of interest equal to the average solution over the whole domain* $\Omega_1 \cup \Omega_2$ *given* $NMAX = 380$, $TOL = 0.01$.

6.3. Distinct parabolic operators in Ω_1 and Ω_2. We modify the problem to consider the case of different diffusion coefficients, and set $\mathcal{L}_1 u = -k_1 \Delta u$ and $\mathcal{L}_2 u = -k_2 \Delta u$. In this case, the right-hand sides and the initial and boundary conditions are chosen so that

$$u_i = \exp\left(-100\left(\frac{x-0.5}{k_i} - 0.25\sin(\pi t)\right)^2 - 100(y - 1 - 0.5\cos(\pi t))^2\right), \quad i = 1, 2.$$

The Gaussian, as well as its trajectory, is now compressed in the y-direction by the factor of $1/k_i$ in Ω_i. The solution for $k_1 = 0.2$ and $k_2 = 1$ is shown in Figure 6.2(b).

The quantities of interest are as above: (a) the average solution in $\Omega_1 \cup \Omega_2$, and (b) the weighted average solution on Γ. The meshes obtained using the adaptive strategy are shown in Figures 6.6 and 6.7, and the estimated error values in Tables 6.6 and 6.7, respectively.

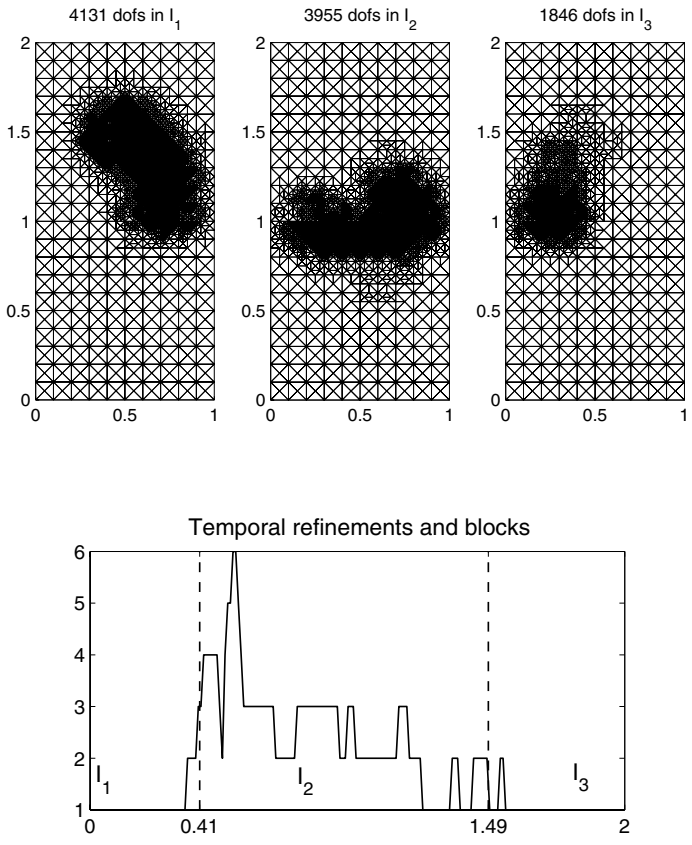

FIG. 6.7. *Subsection* 6.3(b). *Space/time blocks and temporal refinements produced for the quantity of interest equal to the weighted average solution on the interface* Γ *given* $NMAX = 400$, $TOL = 0.05$.

TABLE 6.6

Subsection 6.3(a). *Estimated total errors* $\mathcal{E}_{est}$ *and* $\overline{\mathcal{E}}_{est}$ *for a quantity of interest equal to the average error in the domain, their temporal and spatial components* $\mathcal{E}_t$ *and* $\mathcal{E}_x$, *and the corresponding* L_2*-error* e_Ω *calculated on the original uniform mesh and on the mesh obtained after space-time refinement with* $NMAX = 380$, $TOL = 0.01$.

Mesh (DOF)	$10^4\mathcal{E}_{est}$	$10^4\mathcal{E}_t$	$10^4\mathcal{E}_x$	$10^2\overline{\mathcal{E}}_{est}$	$10^2\overline{\mathcal{E}}_t$	$10^2\overline{\mathcal{E}}_x$	$10^2 e_\Omega$
Original (453)	4.7002	0.0392	4.3080	3.1783	1.9066	1.2717	6.2929
Refined (4071)	−0.0950	−0.0108	−0.0842	0.8988	0.8178	0.0810	0.4668

For both quantities of interest we observe some common features of the refined mesh. Fewer temporal blocks are required to trace the trajectory in Ω_1, where the solution is now compressed relative to the case when $k_1 = k_2 = 1$, and travels closer to the interface. The highly refined region is noticeably thinner in the y-direction in the second block as compared to the other blocks. The error is reduced similarly to the $k_1 = k_2 = 1$ case. Note that in the case of interface refinements there is now less cancelation of error due to lack of symmetry in the solution, and the error $\mathcal{E}$ is higher than before. As before, temporal refinements are concentrated around $t = 0.5$

TABLE 6.7

Subsection 6.3(b). *Estimated total errors* $\mathcal{E}_{est}$ *and* $\overline{\mathcal{E}}_{est}$ *for a quantity of interest defined on the interface, their temporal and spatial components* $\mathcal{E}_t$ *and* $\mathcal{E}_x$*, and the corresponding* L_2*-error* e_Γ *calculated on the original uniform mesh and on the mesh obtained after space-time refinement with* $NMAX = 400$*,* $TOL = 0.05$*.*

Mesh (DOF)	$10^3\mathcal{E}_{est}$	$10^3\mathcal{E}_t$	$10^3\mathcal{E}_x$	$10^2\overline{\mathcal{E}}_{est}$	$10^2\overline{\mathcal{E}}_t$	$10^2\overline{\mathcal{E}}_x$	$10^2 e_\Gamma$
Original (453)	−2.4888	−0.3023	−2.1865	6.3889	4.1615	2.2274	3.5735
Refined (4131)	−0.1630	−0.1698	0.0068	3.2128	3.0366	0.1762	0.3220

and $t = 1.5$, where the speed of the Gaussian peak is highest. In the case of domain errors, more temporal refinements are now required in Ω_2, where the peak is poorly resolved. In the case of interface errors, most refinement occur near $t = 0.5$, where the weighting of the errors is higher. The absolute error $\overline{\mathcal{E}}$ and its components are reduced by a small factor, but sufficiently to reach the global tolerance.

7. Conclusions. We performed an adjoint-based a posteriori analysis for the error in a given quantity of interest of solutions to parabolic problems that are coupled across a common interface. A number of numerical simulations were performed to validate this result in test problems where the exact error could be obtained. As anticipated, the accuracy of the error estimate depends upon the accuracy of the adjoint solution.

A block time-space refinement strategy based on the error representation formula was implemented which takes advantage of our ability to distinguish between temporal and spatial errors. The performance of the algorithm was investigated in the case of a travelling wave-like solution. The block time-space refinement strategy was shown to produce efficient refinements to reduce the errors in a wide range of quantities of interest. Imposing an upper limit on the number of degrees of freedom in a time block provides a useful technique when computational resources are limited.

The extension of this framework to multiphysics systems that are coupled across boundaries whose location is known a priori is a relatively straightforward procedure. For example, coupling between Stokes and Darcy flows implementing the Beavers–Joseph–Saffman condition requires that continuity of the normal component of velocity and the normal component of stress on the interface be enforced. This can be achieved using a similar Lagrange multiplier construction. Further extensions of this approach include the application to deformable boundary such as that which occurs in fluid-solid interactions problems [36].

Acknowledgment. The numerical results presented in sections 5 and 6 were partly obtained using the Oxford e-Research Centre Windows Compute Cluster.

REFERENCES

[1] M. AINSWORTH AND J. T. ODEN, *A posteriori error estimation in finite element analysis*, Comput. Method. Appl. Mech. Engrg., 142 (1997), pp. 1–88.

[2] T. ARBOGAST, L. C. COWSAR, M. F. WHEELER, AND I. YOTOV, *Mixed finite element methods on nonmatching multiblock grids*, SIAM J. Numer. Anal., 37 (2000), pp. 1295–1315.

[3] T. ARBOGAST, G. PENCHEVA, M. F. WHEELER, AND I. YOTOV, *A multiscale mortar mixed finite element method*, Multiscale Model. Simul., 6 (2007), pp. 319–346.

[4] I. BABUŠKA AND W. C. RHEINBOLDT, *A posteriori error estimates for the finite element method*, Int. J. Numer. Meth. Eng., 12 (1978), pp. 1597–1615.

[5] R. BECKER AND R. RANNACHER, *An optimal control approach to a posteriori error estimation in finite element methods*, Acta Numer., 10 (2001), pp. 1–102.

[6] F. Ben Beglacem, *The mortar finite element method with Lagrange multipliers*, Numer. Math., 84 (1999), pp. 173–197.
[7] C. Bernardi, Y. Maday, and A. T. Patera, *A new nonconforming approach to domain decomposition: The mortar element method*, in Nonlinear Partial Differential Equations and Their Applications, Collège de France Seminar, Vol. XI (Paris, 1989–1991), Pitman Res. Notes Math. Ser. 299, Longman Sci. Tech., Harlow, 1994, pp. 13–51.
[8] V. Carey, D. Estep, A. Johansson, M. Larson, and S. Tavener, *Blockwise adaptivity for time dependent problems based on coarse scale adjoint solutions*, SIAM J. Sci. Comput., 32 (2010), pp. 2121–2145.
[9] V. Carey, D. Estep, and S. Tavener, *A posteriori analysis and adaptive error control for multiscale operator decomposition solution of elliptic systems* I: *Triangular systems*, SIAM J. Numer. Anal., 47 (2009), pp. 740–761.
[10] C. Carstensen, *Estimation of higher Sobolev norm from lower order approximation*, SIAM J. Numer. Anal., 42 (2005), pp. 2136–2147.
[11] J. De Hart, G. W. M. Peters, P. J. G. Schreurs, and F. P. T Baaijens, *A three-dimensional computational analysis of fluid-structure interaction in the aortic valve*, J. Biomech., 36 (2003), pp. 103–112.
[12] E. S. Di Martino, G. Guadagni, A. Fumero, G. Ballerini, R. Spirito, P. Biglioli, and A. Redaelli, *Fluid-structure interaction within realistic three-dimensional models of the aneurysmatic aorta as a guidance to assess the risk of rupture of the aneurysm*, Med. Eng. Phys., 23 (2001), pp. 647–655.
[13] W. Dörfler, *A convergent adaptive algorithm for Poisson's equation*, SIAM J. Numer. Anal., 33 (1996), pp. 1106–1124.
[14] K. Eriksson, D. Estep, P. Hansbo, and C. Johnson, *Introduction to adaptive methods for differential equations*, Acta Numer., Cambridge University Press, Cambridge, 1995, pp. 105–158.
[15] K. Eriksson and C. Johnson, *Adaptive finite element methods for parabolic problems* I: *A linear model problem*, SIAM J. Numer. Anal., 28 (1991), pp. 43–77.
[16] K. Eriksson and C. Johnson, *Adaptive finite element methods for parabolic problems* IV: *Nonlinear problems*, SIAM J. Numer. Anal., 32 (1995), pp. 1729–1749.
[17] D. Estep, V. Carey, V. Ginting, S. Tavener, and T. Wildey, *A posteriori error analysis of multiscale operator decomposition methods for multiphysics models*, J. Phys. Conf. Ser., 125 (2008), 012075.
[18] D. Estep, S. Tavener, and T. Wildey, *A posteriori analysis and improved accuracy for an operator decomposition solution of a conjugate heat transfer problem*, SIAM J. Numer. Anal., 46 (2008), pp. 2068–2089.
[19] C. A. Felippa, K. C. Park, and C. Farhat, *Partitioned analysis of coupled mechanical systems*, Comput. Method. Appl. Mech. Engrg., 190 (2001), pp. 3247–3270.
[20] M. Giles and E. Süli, *Adjoint methods for PDEs: A posteriori error analysis and postprocessing by duality*, Acta Numer., 11 (2002), pp. 145–236.
[21] V. Girault, R. Glowinski, H. López, and J.-P Vila, *A boundary multiplier/fictitious domain method for the steady incompressible Navier–Stokes equations*, Numer. Math., 88 (2001), pp. 75–103.
[22] M. Heil, A. Hazel, and J. Boyle, *Solvers for large-displacement fluid-structure interaction problems: Segregated versus monolithic approaches*, Comput. Mech., 43 (2008), pp. 91–101.
[23] M. Heil, A. L. Hazel, and J. A. Smith, *The mechanics of airway closure*, Resp. Physiol. Neurobi., 163 (2008), pp. 214–221.
[24] V. Heuveline and R. Rannacher, *Duality-based adaptivity in the hp-finite element method*, J. Numer. Math., 11 (2003), pp. 95–113.
[25] M. Holst and S. Pollock, *Convergence of goal-oriented adaptive finite element methods for nonsymmetric problems*, arXiv:1108.3660v2.
[26] U. Küttler, M. Gee, C. Förster, A. Comerford, and W. A. Wall, *Coupling strategies for biomedical fluid-structure interaction problems*, Int. J. Numer. Methods Biomed. Eng., 26 (2010), pp. 305–321.
[27] W. J. Layton, F. Schieweck, and I. Yotov, *Coupling fluid flow with porous media flow*, SIAM J. Numer. Anal., 40 (2002), pp. 2195–2218.
[28] H. G. Matthies and J. Steindorf, *Partitioned strong coupling algorithms for fluid-structure interaction*, Comput. Struct., 81 (2003), pp. 805–812.
[29] M. S. Mommer and R. Stevenson, *A goal-oriented adaptive finite element method with convergence rates*, SIAM J. Numer. Anal., 47 (2009), pp. 861–886.
[30] P. Morin, R. H. Nochetto, and K. G. Siebert, *Convergence of adaptive finite element methods*, SIAM Rev., 44 (2002), pp. 631–658.

[31] R. H. Nochetto, K. G. Siebert, and A. Veeser, *Theory of Adaptive Finite Element Methods: An Introduction*, Springer, Berlin, 2009.
[32] R. H. Nochetto, A. Veeser, and M. Verani, *A safeguarded dual weighted residual method*, IMA J. Numer. Anal., 29 (2009), pp. 126–140.
[33] D. Nordsletten, D. Kay, and N. Smith, *A non-conforming monolithic finite element method for problems of coupled mechanics*, J. Comput. Phys., 229 (2010), pp. 7571–7593.
[34] A. Quarteroni and A. Valli, *Domain Decomposition Methods for Partial Differential Equations*, Oxford University Press, New York, 1999.
[35] R. Rannacher, *Adaptive Galerkin finite element methods for partial differential equations*, J. Comput. Appl. Math., 128 (2001), pp. 205–233.
[36] K. G. van der Zee, E. H. van Brummelen, I. Akkerman, and R. de Borst, *Goal-oriented error estimation and adaptivity for fluid-structure interaction using exact linearized adjoints*, Comput. Methods Appl. Mech. Engrg., 200 (2011), pp. 2738–2757.
[37] K. G. van der Zee, E. H. van Brummelen, and R. de Borst, *Goal-oriented error estimation and adaptivity for free-boundary problems: The domain-map linearization approach*, SIAM J. Sci. Comput., 32 (2010), pp. 1064–1092.
[38] W. A. Wall and T. Rabczuk, *Fluid-structure interaction in lower airways of CT-based lung geometries*, Internat. J. Numer. Methods Fluids, 57 (2008), pp. 653–675.
[39] N. Yan and A. Zhou, *Gradient recovery type a posteriori error estimates for finite element approximations on irregular meshes*, Comput. Method. Appl. Mech. Engrg., 190 (2001), pp. 4289–4299.
[40] O. C. Zienkiewicz and J. Z. Zhu, *The superconvergence patch recovery (SPR) and adaptive finite element refinement*, Comput. Method. Appl. Mech. Engrg., 101 (1992), pp. 207–224.
[41] O. C. Zienkiewicz and J. Z. Zhu, *The superconvergent patch recovery and a posteriori error estimates*, Internat. J. Numer. Methods Engrg., 33 (1992), pp. 1331–1364.